ARTICLE IN PRESS

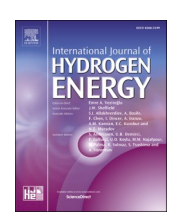
International Journal of Hydrogen Energy xxx (xxxx) xxx

FISEVIER

Contents lists available at ScienceDirect

International Journal of Hydrogen Energy

journal homepage: www.elsevier.com/locate/he



Nickel sulfide nanowire-filled carbon nanotubes as electrocatalysts for efficient hydrogen evolution reaction

Ram Chandra Gotame ^a, Yuba Raj Poudel ^a, Biplav Dahal ^a, Arun Thapa ^a, Christopher Dares ^b, Wenzhi Li ^{a,*}

ARTICLE INFO

Keywords: Hydrogen evolution reaction (HER) Electrocatalyst Overpotential Nickel sulfide Filled carbon nanotubes

ABSTRACT

Developing a cost-effective, efficient, and eco-friendly electrocatalyst made from non-noble materials for the hydrogen evolution reaction (HER) is challenging. This research paper presents an application of the nickel sulfide (Ni₃S₂) nanowires-filled multiwalled carbon nanotubes (CNTs) synthesized on carbon cloth (CC) (Ni₃S₂@CNTs/CC) as an efficient HER electrocatalyst. The performance of Ni₃S₂@CNTs/CC as a working electrode was examined for its hydrogen evolution ability. In a 1.0 M KOH solution, Ni₃S₂@CNTs/CC requires cathodic overpotentials of 381 mV and 549 mV to generate current densities of 10 mA/cm² and 100 mA/cm², respectively. Electrochemical impedance measurements showed a low charge transfer resistance value of 3.3 Ω for Ni₂S₂@CNTs/CC.

The evaluation of the electrochemically active surface area revealed that $Ni_3S_2@CNTs/CC$ has more electrochemical active sites and a higher roughness factor than pristine CC. Most importantly, the current density of $Ni_3S_2@CNTs/CC$ did not significantly degrade after 3000 CV cycles and 12 h of constant HER. These findings suggest that $Ni_3S_2@CNTs/CC$ is a cost-effective, highly functional, and stable electrode material for HER in a strongly alkaline medium.

1. Introduction

According to projections, global energy consumption is expected to reach 30 TW (30 \times 10^{12} Watts) by 2050 [1]. As a result of the high energy demand, the depletion of fossil fuel supply and carbon dioxide emissions from their use are global pressing concerns. Therefore, extensive research has been conducted to develop renewable and clean energy alternatives to address these challenges. Hydrogen (H2) is a promising option among the potential clean energy fuel sources due to its high energy density, carbon emission-free nature, and abundant domestic sources [2–5], which have stimulated interest in hydrogen as an alternative clean energy fuel.

Hydrogen production through biomass pyrolysis is a promising method wherein natural organic materials are heated and gasified at a temperature range of 500–900 $^{\circ}\text{C}$ under 0.1–0.5 MPa pressure [6]. Gasification is also an encouraging technique where specific gasification agents transform biomass into a gaseous mixture, such as CO₂ and H₂ [7]. Other methods, such as biomass combustion, bio-photolysis, steam

reforming, and photo fermentation, are also available for hydrogen production [8]. Although these methods could yield H_2 from 4 g/kg to 190 g/kg feedstock, they face challenges such as catalyst deactivation, costly reactor requirements, and CO_2 emission, limiting their industrial utilization. Furthermore, H_2 production from solar and wind-powered processes is intermittent because they are seasonally dependent. Hence, there is a pressing need for an affordable, emission-free, and industrially applicable technique for green H_2 production.

HER via water electrolysis is considered one of the easiest and cleanest ways to produce pure H_2 , and it is also the most feasible method to produce highly pure H_2 [9–11]. Currently, only a small percentage, around 4 %, of hydrogen produced globally for industrial purposes comes from water electrolysis. The majority, approximately 96 %, is obtained through conventional non-renewable methods [12,13]. The slow kinetics of HER and significant energy loss during the process are the primary reasons for the low production of H_2 through water electrolysis. The standard potential for water electrolysis is 1.23 V; however, the practical potential for water electrolysis is higher than the

E-mail address: Wenzhi.Li@fiu.edu (W. Li).

https://doi.org/10.1016/j.ijhydene.2023.10.171

Received 17 August 2023; Received in revised form 7 October 2023; Accepted 17 October 2023 0360-3199/© 2023 Hydrogen Energy Publications LLC. Published by Elsevier Ltd. All rights reserved.

^a Department of Physics, Florida International University, Miami, FL, 33199, USA

^b Department of Chemistry and Biochemistry, Florida International University, Miami, FL, 33199, USA

^{*} Corresponding author.

theoretical value due to the kinetic barrier [14]. The overpotential is the difference between the experimental and standard potentials for water electrolysis. Fortunately, engineering the catalyst can help reduce the overpotential and make the process more efficient [15]. Platinum (Pt) and Pt-based materials are considered the best electrocatalysts for HER as they require minimal overpotential [16]. However, their high cost and limited availability on Earth hinder their industrial use. Therefore, it is crucial to develop an effective, cost-efficient, and abundantly available HER catalyst to achieve affordable, scalable, and sustainable production of $\rm H_2$.

Non-noble metal-based materials are becoming increasingly popular due to their low cost and easy availability, and nickel (Ni) is one of the most promising options for HER electrocatalysis [17–19]. Because Ni has similar chemical properties to Pt, Ni and Ni-based materials, such as binary, ternary, and composite alloys, have been extensively explored as electrode materials for HER [20,21]. Some of the most notable Ni-based electrode materials include nickel phosphide [22–24], sulfide [25–28], chalcogenide [29,30], and selenides [31–34].

Among Ni-based electrocatalysts, nickel sulfide alloy has demonstrated superior electrocatalysis ability in alkaline environments compared to other binary Ni alloys, and different phases of nickel sulfide have been studied to determine their HER activity [35–37]. Nickel sulfide exists in different phases, and because the HER activity is phase-dependent, considerable attention has been given to exploring the phase-dependent HER activity of nickel sulfide [38–42]. Among its three most stable phases (Ni₃S₂, NiS, and NiS₂), due to its large electrochemically active surface area and high conductivity, Ni₃S₂ has the highest HER electrocatalytic activity [25].

Electrocatalysts must meet certain requirements to catalyze the HER process effectively. They should have many reaction sites, be chemically and mechanically stable, have good electrical conductivity, and be costeffective. The substrate used to load the electrocatalysts should not interfere with their inherent characteristics or cause the loss or overrepresentation of HER activity. Previous research has used glassy carbon electrodes and binder materials like Nafion to load the electrocatalyst materials [43-46]. However, this approach has some limitations, such as hindering the electrocatalytic active sites of the materials, requiring extra material for device fabrication, and increasing the series resistance, which can lead to reduced HER activity. Moreover, creating such electrode materials requires a precisely controlled environment, which can be inconvenient. Carbon cloth (CC) is a superior alternative to glassy carbon for many reasons, including its high flexibility, good conductivity, high mechanical and chemical stabilities, low cost, and abundant availability. CC can also be functionalized with various functional electrocatalysts that can be directly used without modifying or destroying the materials' primordial characteristics as an electrode. Therefore, CC is a suitable substrate (working electrode) alternative for HER electrode materials [47,48].

Combining Ni_3S_2 with carbon nanotubes (CNTs) is expected to have a positive effect on the HER process. Ni_3S_2 alone and its composites have been widely studied for HER [49–56], but there has been no report on using Ni_3S_2 encapsulated inside CNTs for HER. When a material is filled inside a CNT, it becomes more stable and is protected from degradation. Additionally, the filling material can strengthen the CNT and prevent CNT's deformation, making the composite suitable for use in extreme environments, such as strong alkaline solutions. In this work, Ni_3S_2 nanowires encapsulated inside multiwalled CNTs were directly synthesized on CC using a simple one-step chemical vapor deposition process. The synthesized material is termed as Ni_3S_2 @CNTs/CC and has been tested for the first time as the electrode for HER. The Ni_3S_2 @CNTs/CC has shown high efficiency for hydrogen production from HER in a strongly alkaline medium.

2. Experimental

2.1. Reagents and materials

Nickel nanoparticles (Ni NPs) (40 nm, 99.9 %) were purchased from US Research Nanomaterials, Inc. Woven carbon fiber cloth (CC) with a thickness of 330 μ m was purchased from the Fuel Cell Store. Isopropyl alcohol (IPA) was obtained from Fisher Scientific. The precursor for carbon and sulfur was thiophene (C₄H₄S), purchased from Acros Organics. For HER measurements, 1.0 M KOH electrolyte was prepared from potassium hydroxide (\geq 85 %, pellets) purchased from Sigma-Aldrich and mixed with Milli-Q water. All the materials were used as received.

2.2. Material synthesis

Our published work [57] details the synthesis technique of Ni₃S₂@CNTs/CC. Firstly, Ni NPs were mixed with IPA at a concentration of 40 g/L and placed in an ultrasonication bath for 5 min to create a uniform suspension. Next, the catalyst solution was loaded onto small CC pieces of 2 cm × 1.5 cm using the dip-coating method. The catalyst-loaded CC was then heated on a hot plate at 150 °C for 5 min to evaporate the IPA. Afterward, the CC was transferred to a horizontal tube furnace and heated at 600 °C for 30 min with Ar gas flowing at 200 sccm. H₂ flow was then added to the system at 120 sccm for 15 min. Following this, the H₂ flow was stopped, and the system's temperature was raised to the synthesis temperature of 1000 °C. At this point, the Ar flow was increased to 1700 sccm, and the H2 flow (at 120 sccm) was resumed. However, the H2 was flown from a different path (bubbler containing thiophene) to carry the thiophene into the reaction chamber. The synthesis was conducted for 20 min. Finally, the H₂ flow was stopped, the Ar flow was reduced to 200 sccm, and the chamber was cooled to room temperature to collect the samples.

2.3. Morphology and structure characterization techniques

The scanning electron microscopy (SEM) images were acquired using a field emission scanning electron microscope (FESEM) JEOL JSM-6330F and JSM-F100 Schottky FESEM. Transmission electron microscopy (TEM) images were acquired using FEI Tecnai F30 TEM and Tecnai G2 20 U-Twin high-resolution TEM. Siemens Diffraktometer D5000 (Cu K α radiation, $\lambda=1.54$ Å) was used to acquire the X-ray diffraction (XRD) pattern of powder form Ni₃S₂@CNTs.

2.4. Electrochemical measurements

A standard three-electrode system connected to a potentiostat (CH Instruments, Inc. Texas) with a homemade electrochemical cell was used to measure the HER activity of CC and the as-synthesized Ni₃S₂@CNTs/ CC at room temperature. All the electrocatalytic measurements were evaluated in a strongly alkaline 1.0 M KOH solution (electrolyte). The reference and counter electrodes used in the experiment were Ag/AgCl (1 M Na₂SO₄) and graphite rod, respectively. Ar gas at a constant flow rate was purged into the electrolyte 20 min before starting the measurement and during all the electrochemical measurements to degas the system. All the potentials reported in this paper are converted to a reversible hydrogen electrode (vs. RHE) using the equation E (V vs. RHE) = E (V vs. Ag/AgCl) + 0.2 V + 0.059 \times pH (pH = 14.0). Linear sweep voltammetry (LSV) was performed at a scan rate of 5 mV/s. Because of the ohmic resistance of the electrolyte, the as-measured current would not reflect the intrinsic behavior of the electrocatalyst. To solve the problem, 100 % iR correction was applied to the measured LSV by measuring the electrolyte resistance (R_s) from electrochemical impedance spectroscopy (EIS). EIS experiments were performed at a frequency range (high to low) from 100 kHz to 0.1 Hz. The as-obtained EIS data were fitted using the same CHI software. Tafel parameters were

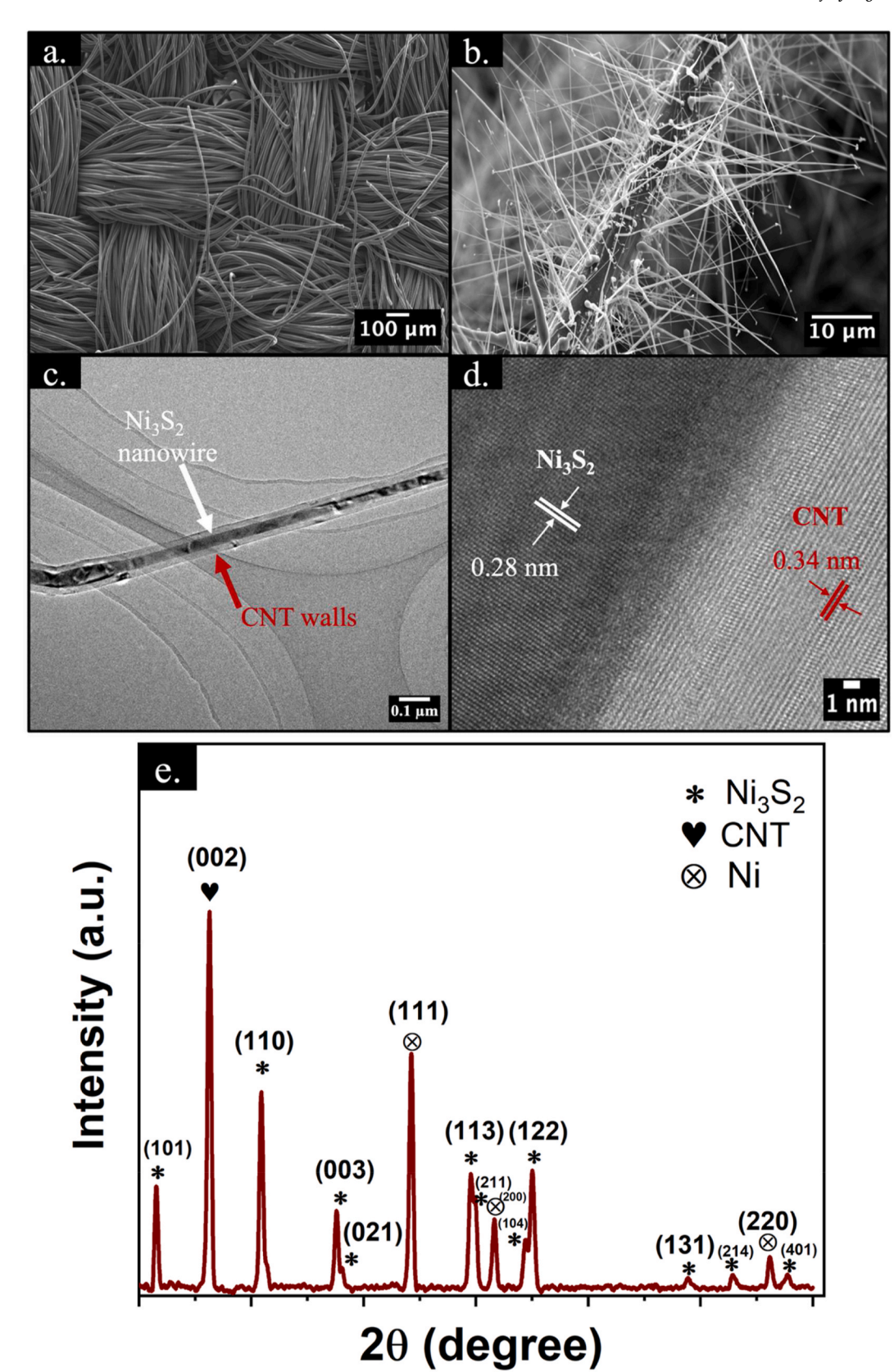


Fig. 1. (a) Low magnification SEM image of woven CC. (b) High magnification SEM image showing Ni_3S_2 @CNTs synthesized on CC. (c) Low magnification TEM image of a single Ni_3S_2 @CNT showing the continuous Ni_3S_2 nanowire filled inside the CNT. (d) High-resolution TEM image of a Ni_3S_2 @CNT showing highly graphitized CNT walls and the crystalline Ni_3S_2 core. (e) X-ray diffraction pattern of powder Ni_3S_2 @CNTs.

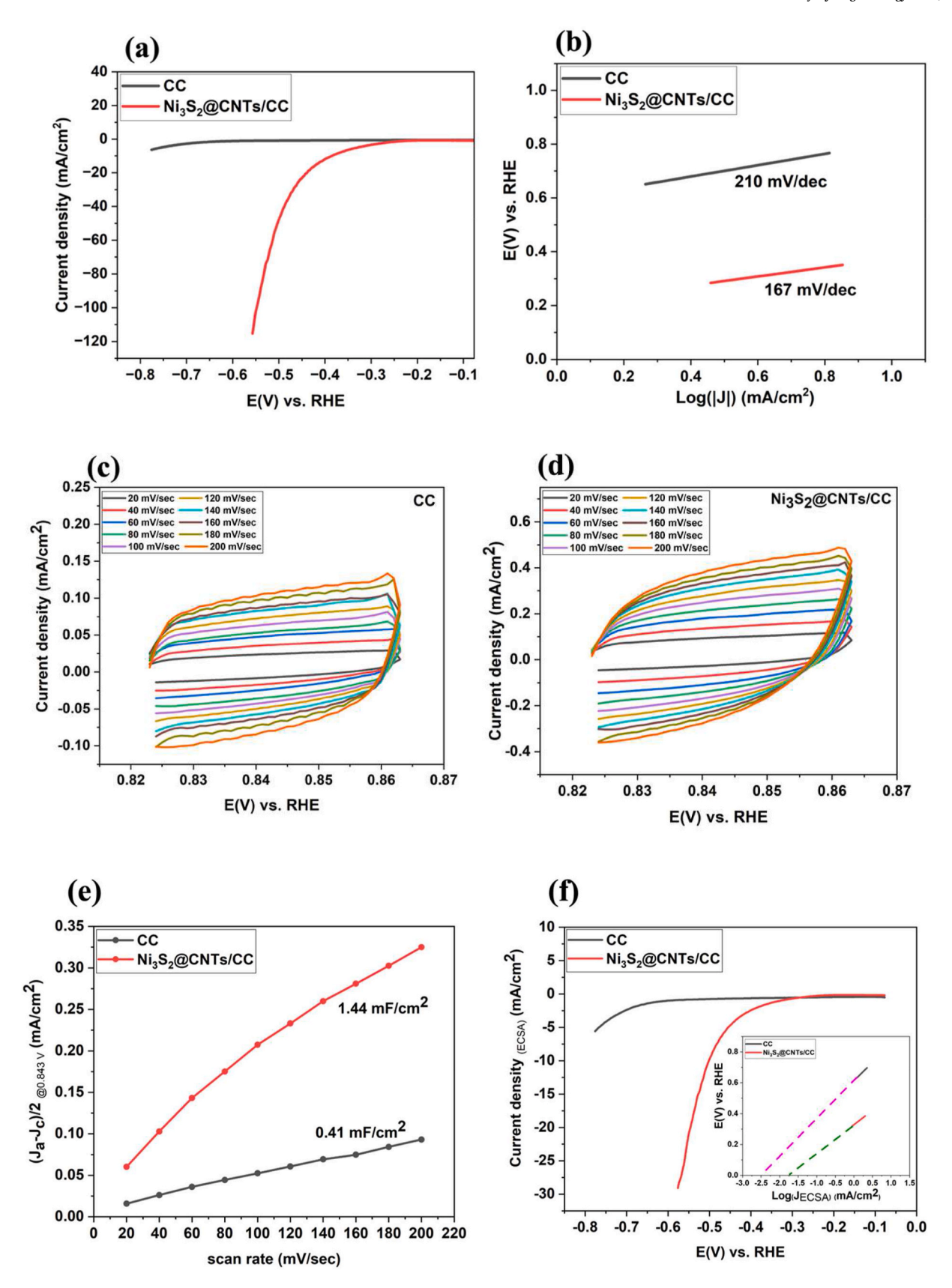


Fig. 2. (a) Linear sweep voltammograms of pristine CC and $Ni_3S_2@CNTs/CC$ (normalized to geometrical surface area). (b) Corresponding Tafel plots of CC and $Ni_3S_2@CNTs/CC$. (c), (d) Cyclic voltammograms of pristine CC and $Ni_3S_2@CNTs/CC$ used for calculating C_{dl} . (e) Scan rate dependence of the current densities of pristine CC and $Ni_3S_2@CNTs/CC$. (f) Linear sweep voltammetry normalized to ECSA. Inset: ECSA normalized Tafel extrapolation for ECSA normalized exchange current density.

calculated based on the standard Tafel equation, $\eta=a+b Log(J)$, where $\eta(V)$ represents the applied overpotential, $J(mA/cm^2)$ the resulting current density, b(V/dec) the Tafel slope and a(V) the intercept. The durability of $Ni_3S_2@CNTs/CC$ was measured using chronoamperometry at a constant potential for 12 h. The cyclic stability test was conducted using cyclic voltammetry (CV) using the same sample for the 1st and the 2nd 1500 CV cycles. For measuring the electrochemical active surface area (ECSA), double layer capacitance (Cdl) was calculated by performing CV scans in the non-faradaic potential region from 20 mV/s to 200 mV/s at 20 mV/s intervals. Initially, all current values are normalized to the geometric surface area of the respective electrodes (current density). Subsequently, they are further normalized to the calculated ECSA. Electrodes and the electrochemical system were activated by performing at least 15 CV cycles at a scan rate of 50 mV/s before starting the electrochemical measurement.

3. Results and discussion

3.1. Physical characterization of the catalysts

Fig. 1(a) displays an SEM image of the pristine CC, which consists of a stack of carbon fiber threads that can be loaded with Ni NPs. Fig. 1(b) shows the SEM image of Ni₃S₂@CNTs that have been synthesized onto the CC substrate. SEM inspection reveals that the Ni₃S₂@CNTs are strongly connected to the carbon threads, and the vast majority of the Ni NPs have participated in the growth of the Ni₃S₂@CNTs. A layer of Ni₃S₂@CNTs, with a length of 20-30 μm, covers the CC substrate. Fig. 1 (c) shows a single CNT that has been entirely filled with Ni₃S₂ nanowire. Most of the Ni₃S₂@CNTs appear straight, while some are curved. Usually, Ni₃S₂@CNTs are slightly tapered, with the thicker end (the root) commonly sealed with a sphere of carbon-encapsulated nickel sulfide. Fig. 1(d) displays a high-resolution TEM image of a Ni₃S₂@CNT that demonstrates the CNT walls' high crystallinity, with a lattice spacing of 0.34 nm, corresponding to the (002) plane of graphitic carbon. The lattice separation of 0.28 nm found in the filler material matches well with the d-spacing of (110) plane of rhombohedral Ni₃S₂, a heazlewoodite phase (a = 5.745 Å and c = 7.135 Å). Further, XRD measurement was performed on the powder form Ni₃S₂@CNTs and shown in Fig. 1 (e). The diffraction patterns at 2θ values of 21.75° , 31.10° , 37.77° , 38.27° , 49.73° , 50.12° , 54.61° , 55.16° , 69.27° , 73.04° , and 77.89° correspond to (101), (110), (003), (021), (113), (211), (104), (122), (131), (214), and (401) planes of rhombohedral Ni₃S₂. The appearance of a diffraction peak at a 20 value of 26.36° represents the (002) plane of CNT. The three peaks at 20 values of 44.50°, 51.84°, and 76.36° correspond to the (111), (200), and (220) planes of unreacted nickel crystal remained at the root of Ni₃S₂@CNTs. The specific surface area (BET) of the CC and Ni₃S₂@CNTs/CC was measured to be 21.7 m²/g and 26.6 m²/g, respectively. The synthesis of Ni₃S₂@CNTs on CC led to a slight increase in the specific surface area. Additional information regarding the Ni₃S₂@CNTs' comprehensive structural analysis and other physical characteristics can be found in our earlier work [57]. The SEM images of Ni_3S_2 @CNTs post-HER testing are shown in ESI Figure S1 (c)-(e). The low-magnification SEM image (Figure S1(c)) reveals that many Ni₃S₂@CNTs collapsed onto the CC while the rest are still freely sticking out of the CC. The collapsing of Ni₃S₂@CNTs on CC could be from the wetting effect of free-standing CNTs [58]. The high-magnification SEM images (Figures S1(d) and (e)) of the single Ni₃S₂@CNTs reveal that the Ni₃S₂ nanowires are still encapsulated in the CNTs even after the HER test, indicating that the Ni₃S₂ nanowires are well protected by the CNTs during the HER test. The robust and enduring nature of Ni₃S₂@CNTs made the HER process stable (see the electrocatalysis performance towards HER below).

3.2. Electrocatalysis performance towards HER

The as-synthesized Ni₃S₂@CNTs/CC was used as a working electrode

to investigate its catalytic activity towards HER without modification. Fig. 2(a) shows the LSV (normalized to geometrical surface area) of Ni₃S₂@CNTs/CC and pristine CC recorded at a scan rate of 5 mV/s. It is evident from the polarization curve that pristine CC shows inferior HER activity, while Ni₃S₂@CNTs/CC exhibits significant HER activity with high current density. Quantitatively, Ni₃S₂@CNTs/CC requires overpotentials of $-381\ mV$ and $-137\ mV$ to generate current densities of 10 mA/cm^2 (η_{10}) and 1 mA/cm^2 (onset overpotential, η_1), respectively. The current density obtained at the maximum applied potential for CC was less than 7.5 mA/cm². It is important to note that the onset overpotential of pristine CC is -500 mV, 3.6 times higher than that of the Ni₃S₂@CNTs/CC. Also, the LSV of Ni₃S₂@CNTs/CC shows that a current density of 100 mA/cm^2 can be achieved at an overpotential of -549 mV. Therefore, we conclude that the Ni₃S₂-filled CNTs synthesized on CC enhance the HER activity by facilitating the electron transfer process, allowing for easy electrolyte diffusion, and increasing the reaction sites.

To investigate the kinetics of the HER, the Tafel plot (Fig. 2(b)) was derived from corresponding LSV (normalized by geometrical surface area) curves. This plot reveals the rate-determining step (RDS) during HER. Slope values of $\sim 30 \text{ mV/decade}$, $\sim 40 \text{ mV/decade}$, and $\sim 120 \text{ mV/decade}$ decade of a Tafel plot indicate the Heyrovsky, Tafel, and Volmer as RDS, respectively, during the HER process. The Tafel slope of Ni₃S₂@CNTs/ CC (167 mV/dec) is smaller than that of CC (210 mV/dec). A Tafel slope of >120 mV/dec in an alkaline medium primarily indicates that the water dissociation step controls the reaction, and the RDS is the electron transfer reaction (i.e., the Volmer step, [59,60]. This result agrees with the electrochemical process in alkaline conditions, where the Volmer step is the RDS [61,62]. The exchange current density (J₀), which represents the reaction rate under equilibrium conditions ($\eta = 0$), was obtained by Tafel extrapolation for CC and Ni₃S₂@CNTs/CC (Figure S1 (a)). It was found to be 6.3×10^{-2} mA/cm² for Ni₃S₂@CNTs/CC, which is 63 times higher than 1×10^{-3} mA/cm² of CC. Since the increase in J_0 value indicates that the corresponding material is efficient in producing hydrogen on the surface [63], therefore, the Ni₃S₂@CNTs/CC is more efficient than CC in producing hydrogen on the surface.

The CNT shells of the Ni₃S₂@CNTs play dual roles in the overall HER process. The CNT layers can catalyze the electrolyte, electrochemically allowing the electrolyte to reach the active filler material (Ni₃S₂), while concurrently protect the filler material. Specifically, the outer layer of CNTs acts as a protective shield, effectively shielding the electrochemically active Ni₃S₂ from direct contact with the electrolyte, preventing the loss of active Ni₃S₂ material. This enables the efficient HER process to continue for an extended period of operation. Moreover, the encapsulated nickel sulfide nanowire can significantly increase the adsorption energy of hydrogen atoms on the CNTs by improving the electrical conductivity of the CNT layers [64]. The H₂O molecules in the electrolyte were first adsorbed to the active sites of CNT (C atom). Subsequently, these H2O molecules are transferred to the filler material (Ni₃S₂) through a reactive process driven by the transfer of electrons originating from the CNT [65]. Furthermore, the nanopores or defects within the carbon nanotube layer can provide a pathway for the diffusion of electrolyte [66] so the electrolyte can reach the Ni₃S₂, which will facilitate the HER process. Due to the favorable adsorption of OH- and the recombination of H⁺ into H₂ at the active C atom of CNT and Ni₃S₂ sites, Ni₃S₂@CNTs efficiently catalyze the decomposition of H₂O into OH⁻ and, consequently, the production of H₂. As a result, a synergistic catalytic process occurs, wherein Ni₃S₂@CNTs collectively enhance H₂ generation through the HER, as described by the following equations

$$H_2O + M + e^- \rightarrow MH_{ads} + OH^ MH_{ads} + H_2O + e^- \rightarrow H_2 + M + OH^ MH_{ads} + MH_{ads} \rightarrow 2 M + H_2$$
 $(M = catalyzer, H_{ads} = adsorbed hydrogen)$

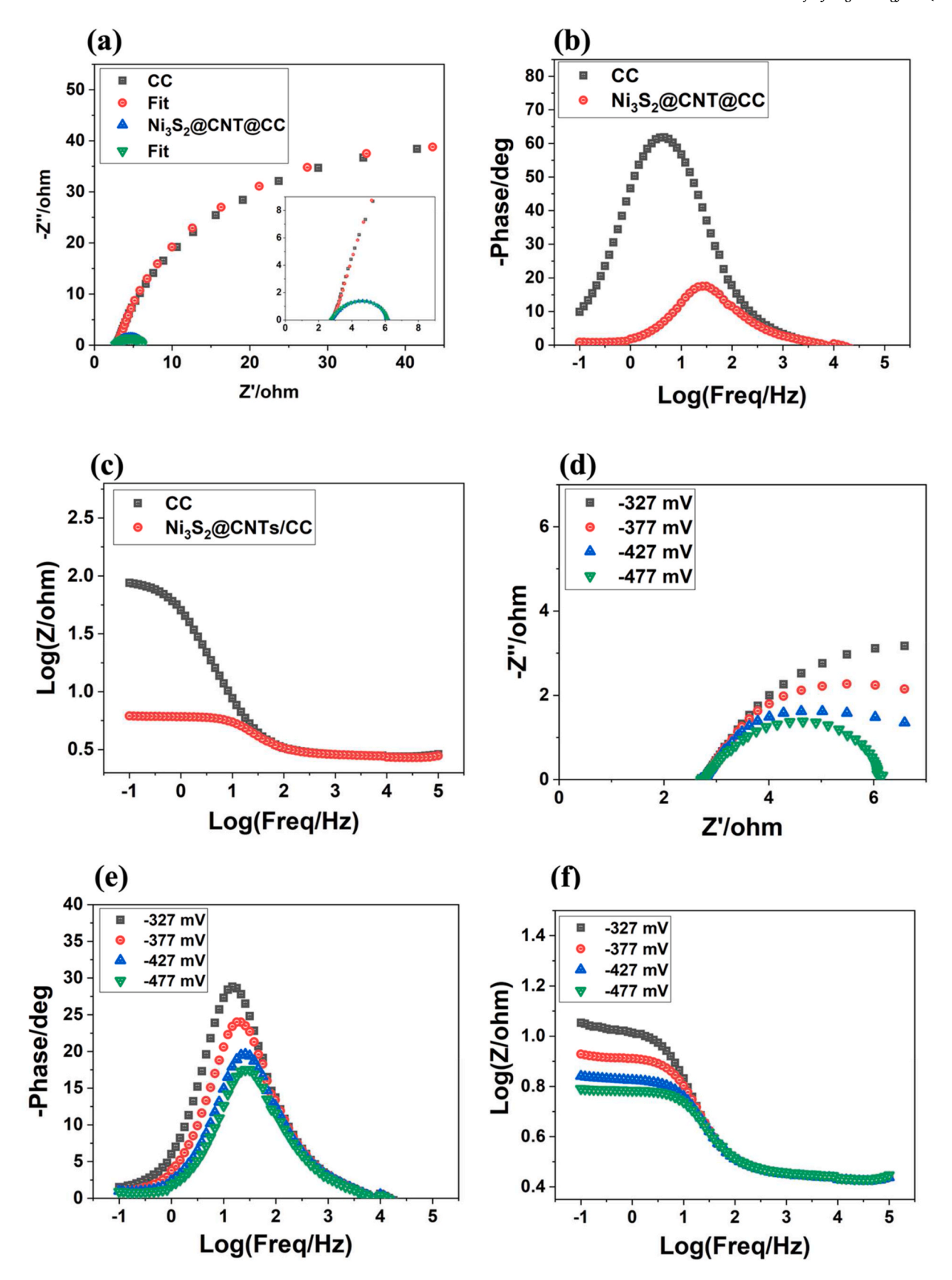


Fig. 3. Nyquist plot of (a) pristine CC and Ni₃S₂@CNTs/CC at -477 mv. Inset: zoom-in area with smaller frequency. (b), (c) Bode plots of pristine CC and Ni₃S₂@CNTs/CC. (d)-(f) Potential dependent Nyquist and Bode plots of Ni₃S₂@CNTs/CC.

To accurately evaluate the relative HER activity, the electrochemically active surface area (ECSA) was measured for both pristine CC and Ni₃S₂@CNTs/CC. Because the charging current (i_c) is equal to the product of the electrochemical double layer capacitance (C_{dl}) and the scan rate (ν), as in equation (1) [68,69].

$$i_c = \nu C_{dl}$$
 (1)

 C_{dl} can be estimated by calculating the slope of the i_c vs. ν graph. Accordingly, the ECSA is given by equation (2).

$$ECSA = \frac{C_{dl}}{C_{c}}$$
 (2)

where C_s is the specific capacitance.

So, a graph of $(\frac{J_a-J_c}{2})$ at mid-potential vs. scan rates was plotted, and the slope corresponding to C_{dl} was determined. J_a and J_c represent the anodic and cathodic current density, respectively.

Fig. 2(c) and (d) show the CV measurements of the Ni₃S₂@CNTs/CC and CC recorded in the non-faradaic potential region at scan rates 20-200 mV/sec in an interval of 20 mV/sec. The scan rate dependence of the current densities $(\frac{J_a-J_c}{2})$ at mid-potential of 0.843 V for pristine CC and Ni₃S₂@CNTs/CC is shown in Fig. 2(e). Based on Fig. 2(e), the C_{dl} of pristine CC and Ni₃S₂@CNTs/CC is 0.41 mF/cm² and 1.44 mF/cm², respectively. To quantitatively compare the ECSAs of Ni₃S₂@CNTs/CC and CC, a specific capacitance value of 0.118 mF/cm² [70] was used in equation (2). The calculated ECSAs for Ni₃S₂@CNTs/CC and CC are 12.2 cm⁻² and 3.47 cm⁻², respectively. The ECSA of the Ni₃S₂@CNTs/CC is 3.51 times that of pristine CC. We believe that the microstructure of Ni₃S₂ nanowire-filled CNTs grown on CC increases the ECSA of Ni₃S₂@CNTs/CC, promoting the HER activity afterward. Furthermore, the ratio of ECSA to the geometric area can describe the roughness factor (RF) [69]. Because the ECSA is higher for Ni₃S₂@CNTs/CC, it is evident that the Ni₃S₂@CNTs/CC possess a much higher surface roughness than pristine CC. The calculated RF was 1.15 for CC and 4.06 for Ni₃S₂@CNTs/CC, respectively. Therefore, the increased roughness factor of Ni₃S₂@CNTs/CC is another determinant responsible for its better HER catalytic activity than CC. Also, the ECSA was used to obtain the ECSA normalized current density, from which the ECSA normalized exchange current density was calculated [71,72]. The linear sweep voltammetry normalized to the ECSA (Fig. 2(f)) shows that Ni₃S₂@CNTs/CC has much higher current density than CC at the same potential, indicating that Ni₃S₂@CNTs/CC has significantly better intrinsic HER activity than CC. Furthermore, the exchange current density normalized to ECSA has been calculated using the ECSA normalized Tafel extrapolation (Fig. 2(f), inset). The ECSA normalized exchange current density for CC and Ni₃S₂@CNTs/CC is found to be 3.1 \times 10⁻³ mA/cm² and 1.77 \times 10⁻² mA/cm², indicating that the enhanced HER of the Ni₃S₂@CNTs/CC is mainly from the catalyzing ability of the Ni_3S_2 @CNTs. Thus, according to the above observations, the substantial improvement of intrinsic HER activity of Ni₃S₂@CNTs/CC can be attributed to the synthesized Ni₃S₂@CNTs on CC.

During the HER process, EIS measurement was used to determine the electron transfer kinetics of pristine CC and Ni₃S₂@CNTs/CC. The electrode impedance indicates the resistance encountered while transferring charges, and a smaller impedance value suggests a more favorable HER process. Specifically, a smaller charge transfer resistance (R_{ct}) represents better HER ability. The kinetics of charge transfer for pristine CC and Ni₃S₂@CNTs/CC was investigated using EIS at an overpotential of -477 mV. The corresponding Nyquist and Bode plots are presented in Fig. 3. As shown in the figure, a semicircle in the high to low-frequency region can describe the charge transfer process (charge transfer resistance) for both CC and Ni₃S₂@CNTs/CC. The charge transfer resistance (R_{ct}) is related to the diameter of the semicircular portion of the Nyquist diagrams, and a smaller diameter means a faster electron transfer process and, ultimately, better HER activity [73,74]. Fig. 3(a) shows that the R_{ct} for Ni₃S₂@CNTs/CC is much smaller than that of pristine CC. To

Table 1 Comparison of R_{ct} from EIS of different samples for HER.

Sample	R _{ct} (ohm)	Electrolyte	Ref.
Ni ₃ S ₂ @CNTs/CC	3.3 @ -477 mV 29.21 @ -200 mV	1 М КОН	This work.
Ni NP-carbon paper	>400 @ -200 mV	1 M KOH	[75]
MWCNT/GC	>2000 @ -200 mV	0.1 M KCl	[78]
MWCNTs@CU	>2500 @ -100 mV	$0.5~\mathrm{M~H_2SO_4}$	[79]
Ni ₃ S ₂ (55 %)/MWCNT-NC	244 @ -400 mV	$1~\mathrm{M~KOH}$	[76]

Table 2Comparison of the overpotential of different samples for HER.

Samples	Overpotential (mV)	Electrolyte	Ref.
Ni ₃ S ₂ @CNTs/CC	381 mV @ 10 mA/cm ²	1 М КОН	This work.
MWCNTs	~600 mV @ 10 mA/cm ²	0.5 M H ₂ SO ₄	[78]
MWCNTs	686 mV @ 10 mA/cm ²	0.5 M H ₂ SO ₄	[80]
1/MWCNT	571 mV @ 10 mA/cm ²	$0.5 \text{ M H}_2\text{SO}_4$	[81]
iMWCNTs	440 mV @ onset	0.5 M H ₂ SO ₄	[82]
Ni ₃ S ₂ (55 %)/MWCNT- NC	400 mV @ 1.2 mA/cm ²	1 М КОН	[76]

quantitatively estimate the R_{ct} , the measured EIS data were fitted using a Randles circuit (Figure S1(b), inset), which includes a charge transfer resistance (R_{ct}) in parallel with a series combination of double-layer capacitance (C_{dl}) and constant phase element (CPE) and then jointly in series with a solution resistance (R_s). The fitted results show that the working electrodes (CC and Ni $_3$ S $_2$ @CNTs/CC) exhibited similar solution resistance ($R_s=2.6~\Omega$), specifying identical reaction conditions. The fitted R_{ct} of pristine CC at the same overpotential of -477~mV was 82.2 Ω , whereas that of Ni $_3$ S $_2$ @CNTs/CC was 3.3 Ω . The lower charge transfer resistance of Ni $_3$ S $_2$ @CNTs/CC compared to pristine CC is indicative of better HER ability.

The synthesized Ni₃S₂@CNTs facilitate the charge transfer process in the electrolyte due to their smaller charge transfer resistance. To confirm that the synthesized Ni₃S₂@CNTs are responsible for the measured HER activity, we obtained the R_{ct} at the same overpotential (-200 mV vs. RHE) as used for measuring Ni NPs on CC [75] (Figure S1 (b)). The R_{ct} obtained for Ni₃S₂@CNTs/CC is much smaller (29.21 Ω) compared to that of Ni NPs on CC ($>400 \Omega$). Additionally, the R_{ct} of multi-walled CNTs is higher than that of Ni₃S₂@CNTs/CC (Table 1). The overpotential previously reported for multiwalled carbon nanotubes is also higher than for Ni₃S₂@CNTs/CC (Table 2). Therefore, we believe that the HER activity of our material is due to the harmonization of Ni₃S₂@CNTs microstructure synthesized on CC rather than just Ni NPs or CNTs (if any remaining Ni NPs exist). Furthermore, the HER parameters obtained for Ni₃S₂@CNTs/CC are comparable or superior to the best-matched work reported previously [76] (Tables 1 and 2).

Fig. 3(b) and (c) display Bode plots for pristine CC and Ni₃S₂@CNTs/CC. To calculate the relaxation time, we used the plot of Log (Frequency/Hz) *vs.* -phase/degree and found the reciprocal of the frequency/Hz for the -phase/degree peak. Comparing the two samples, Ni₃S₂@CNTs/CC had a lower relaxation time (0.031 s) than pristine CC (0.21 s) and exhibited a faster electron transfer rate at the lowest frequency (0.1 Hz) due to its lower impedance (|Z|) value.

A potential dependent EIS study was executed to illustrate the

 $\label{eq:continuous_section} \textbf{Table 3} \\ R_s, \ R_{ct}, \ Z, \ C_{dl,} \ \text{and relaxation time from EIS best fit of Ni}_3S_2@CNTs/CC \ \text{at different cathodic overpotentials.}$

η (mV)	$R_s(\Omega)$	$R_{ct}(\Omega)$	$ Z (\Omega)$	$C_{dl} (mF/cm^2)$	Relaxation Time (sec)
-327	2.6	7.9	2.85	1.15	0.068
-377	2.6	5.5	2.52	1.13	0.046
-427	2.6	4.0	2.31	1.12	0.038
-477	2.6	3.3	2.20	1.12	0.031

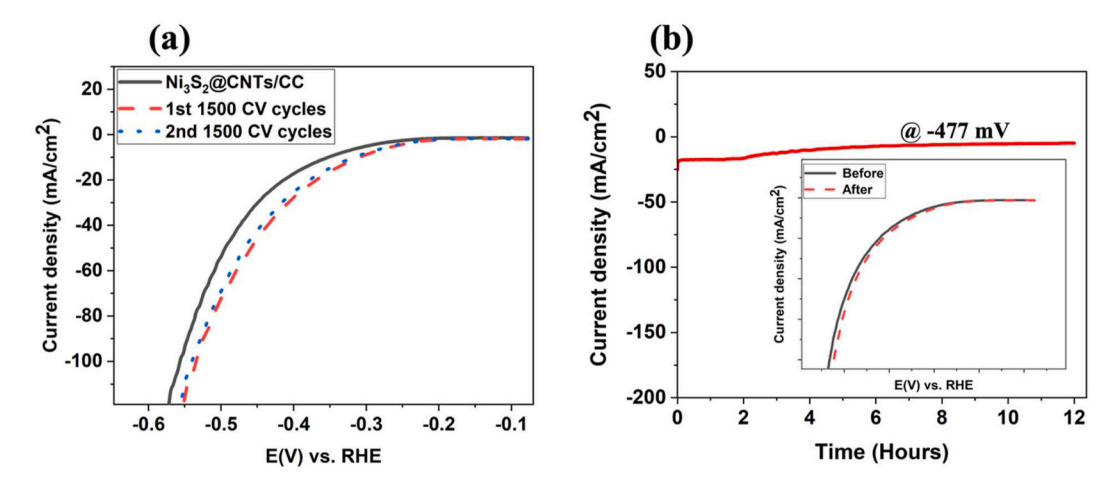


Fig. 4. (a) LSV curve of Ni₃S₂@CNTs/CC before and after the 1st and 2nd 1500 CV cycles at a 30 mV/sec scan rate. (b) Time-dependent current density at -477 mV for 12 h. The inset shows the LSV curve of Ni₃S₂@CNTs/CC before and after 12 h of constant chronoamperometric measurement.

relative enhancement of HER activity of Ni₃S₂@CNTs/CC. Fig. 3(d)-(f) show the Nyquist and Bode plots of Ni₃S₂@CNTs/CC in the potential scope of -327 mV to -477 mV. The R_s , R_{ct} , and C_{dl} were obtained by fitting the corresponding Nyquist plot and listed in Table 3. We observed that the diameter of the semicircle decreases with the increase of the cathodic overpotentials. Bode plots also showed that the phase angle and total impedance become smaller at higher applied cathodic potentials. Also, the relaxation time decreases with increased applied cathodic overpotential. The decreased R_{ct}, phase angle, impedance, and relaxation time with the increasing cathodic overpotential denotes superior hydrogen evolution at a higher applied bias. Furthermore, visual observation also confirmed that hydrogen bubble evolution is more vigorous at the electrode surface in LSV towards higher cathodic overpotentials. The decreased value of charge transfer resistance and relaxation time with increasing overpotentials in Nyquist and Bode plots could be attributed to the porous structure on the electrode surface and the excellent kinetics of the HER process by Ni₃S₂@CNTs/CC [77]. The experimental results indicate that Ni₃S₂@CNTs/CC is an efficient electrode material for HER electrocatalysis in a strongly alkaline solution.

For commercial use, it is important for a catalyst to be not only active but also stable and durable. To test the long-term stability of Ni $_3$ S $_2$ @CNTs/CC, a total of 3000 CV cycles in the potential range of 0.223 V to -0.427 V vs. RHE at a scan rate of 30 mV/sec was performed. The LSV curves of Ni $_3$ S $_2$ @CNTs/CC before and after the 1st and 2nd 1500 CV cycles were compared, as shown in Fig. 4(a). It can be clearly seen from the LSV that Ni $_3$ S $_2$ @CNTs/CC is significantly stable for more than 3000 CV cycles, indicating its excellent stability as an electrocatalyst for HER.

The durability of Ni₃S₂@CNTs/CC was tested using the chronoamperometric technique for 12 h at a constant potential of -477~mV. Throughout the entire test, there was significant H₂ bubbling at the surface of Ni₃S₂@CNTs/CC. Fig. 4(b) shows the time-dependent current density (i-t curve) at constant potential and LSV curves (inset) of Ni₃S₂@CNTs/CC before and after 12 h of constant (i-t) measurement. The current density was almost constant for 12 h, with only a slight decrease after $\sim\!2.5$ h. The LSV curve (Fig. 4(b), inset) after 12 h showed that the overpotential needed to provide 10 mA/cm² of current density was almost identical, indicating the excellent durability of Ni₃S₂@CNTs/CC. Furthermore, no significant degradation in the catalytic activity of Ni₃S₂@CNTs/CC is also supported by the EIS and ECSA measurements (Figure S2 (a)–(c), Table S1) after the 12-h test. These results suggest that Ni₃S₂@CNTs/CC is an efficient, stable, and durable electrocatalyst for HER in a strong alkaline solution.

4. Conclusion

In summary, Ni_3S_2 nanowires-filled carbon nanotubes were synthesized using a simple one-step CVD method on CC substrates. The electrochemical hydrogen evolution ability of the synthesized Ni_3S_2 @CNTs was investigated and compared with pristine CC under strongly alkaline condition (1.0 M KOH) by employing LSV, CV, and EIS techniques. The stability and durability of Ni_3S_2 @CNTs/CC were also investigated. The results showed that Ni_3S_2 @CNTs/CC has superior HER performance, including higher stability, higher durability, higher electrochemical active surface area, lower charge transfer resistance, lower impedance, and lower relaxation time than pristine CC. It is worth mentioning that few materials demonstrate a better HER property in alkaline solution, and Ni_3S_2 @CNTs/CC stood out as one of the few electrode materials for cost-effective hydrogen evolution reactions.

Declaration of competing interest

The authors declare that they have no known competing financial interests or personal relationships that could have appeared to influence the work reported in this paper.

Acknowledgments

This work is supported by the National Science Foundation under grants 1506640, 2134375, and 2213923. We thank Dr. J. Su and Dr. Y. H. Gao (Huazhong University of Science and Technology, Wuhan, Hubei, P. R. China) for their help with the TEM experiment. The authors would also like to acknowledge the SEM and XRD experiment support from the Advanced Materials Engineering Research Institutes (AMERI) at Florida International University (FIU).

Appendix A. Supplementary data

Supplementary data to this article can be found online at https://doi.org/10.1016/j.ijhydene.2023.10.171.

References

- Berry JJ, van de Lagemaat J, Al-Jassim MM, Kurtz S, Yan Y, Zhu K. Perovskite photovoltaics: the path to a printable terawatt-scale Technology. ACS Energy Lett 2017;2(11):2540-4.
- [2] Pareek A, Dom R, Gupta J, Chandran J, Adepu V, Borse PH. Insights into renewable hydrogen energy: recent advances and prospects. Mater Sci Energy Technol 2020; 3:319–27.
- [3] Joya KS, Joya YF, Ocakoglu K, van de Krol R. Water-splitting catalysis and solar fuel devices: artificial leaves on the move. Angew Chem Int Ed 2013;52(40): 10426–37.

- [4] Abbas MK, Hassan Q, Tabar VS, Tohidi S, Jaszczur M, Abdulrahman IS, Salman HM. Techno-economic analysis for clean hydrogen production using solar energy under varied climate conditions. Int J Hydrogen Energy 2023;48(8): 2929–48
- [5] Hassan Q, Sameen AZ, Salman HM, Jaszczur M, Al-Jiboory AK. Hydrogen energy future: advancements in storage technologies and implications for sustainability. J Energy Storage 2023;72:108404.
- [6] Muradov N. Emission-free fuel reformers for mobile and portable fuel cell applications. J Power Sources 2003;118(1):320–4.
- [7] Ahmed TY, Ahmad MM, Yusup S, Inayat A, Khan Z. Mathematical and computational approaches for design of biomass gasification for hydrogen production: a review. Renew Sustain Energy Rev 2012;16(4):2304–15.
- [8] Agyekum EB, Nutakor C, Agwa AM, Kamel S. A critical review of renewable hydrogen production methods: factors affecting their scale-up and its role in future energy generation. Membranes (Basel) 2022;12(2).
- [9] Walter MG, Warren EL, McKone JR, Boettcher SW, Mi Q, Santori EA, Lewis NS. Solar water splitting cells. Chem Rev 2010;110(11):6446–73.
- [10] Dresselhaus MS, Thomas IL. Alternative energy technologies. Nature 2001;414 (6861):332–7.
- [11] Buslaev G, Lavrik A, Lavrik A, Tcvetkov P. Hybrid system of hydrogen generation by water electrolysis and methane partial oxidation. Int J Hydrogen Energy 2023; 48(63):24166–79.
- [12] Shiva Kumar S, Himabindu V. Hydrogen production by pem water electrolysis a review. Mater Sci Energy Technol 2019;2(3):442–54.
- [13] Balat M. Possible methods for hydrogen production. Energy Sources, Part A Recovery, Util Environ Eff 2008;31(1):39–50.
- [14] Applied-Chemistry-a-Texbook-for-Engineris-Technologyist_1539670026".
- [15] Wang S, Lu A, Zhong C-J. Hydrogen production from water electrolysis: role of catalysts. Nano Converg 2021;8(1):4.
- [16] Li C, Baek J-B. Recent advances in noble metal (Pt, Ru, and Ir)-Based electrocatalysts for efficient hydrogen evolution reaction. ACS Omega 2020;5(1): 31–40.
- [17] Miles MH, Thomason MA. Periodic variations of overvoltages for water electrolysis in acid solutions from cyclic voltammetric studies. J Electrochem Soc 1976;123 (10):1459.
- [18] Bu X, Liang X, Bu Y, Quan Q, Meng Y, Lai Z, Wang W, Liu C, Lu J, Lawrence Wu C-M, Ho JC. NiMo@C3N5 heterostructures with multiple electronic transmission channels for highly efficient hydrogen evolution from alkaline electrolytes and seawater. Chem Eng J 2022;438:135379.
- [19] Jeghan SMN, Kim D, Lee Y, Kim M, Lee G. Designing a smart heterojunction coupling of cobalt-iron layered double hydroxide on nickel selenide nanosheets for highly efficient overall water splitting kinetics. Appl Catal, B 2022;308:121221.
- [20] Hu C, Lv C, Zeng N, Liu A, Liu Y, Hu L, Li P, Yao Y, Cai J, Tang T. Recent advances in Ni-based electrocatalysts for hydrogen evolution reaction. Energy Technol 2023; 11(1):2201048.
- [21] Anantharaj S, Kundu S, Noda S. Progress in nickel chalcogenide electrocatalyzed hydrogen evolution reaction. J Mater Chem A Mater 2020;8(8):4174–92.
- [22] Ge Z, Fu B, Zhao J, Li X, Ma B, Chen Y. A review of the electrocatalysts on hydrogen evolution reaction with an emphasis on Fe, Co and Ni-based phosphides. J Mater Sci 2020;55(29):14081–104.
- [23] Xiong L, Wang B, Cai H, Hao H, Li J, Yang T, Yang S. Understanding the doping effect on hydrogen evolution activity of transition-metal phosphides: modeled with Ni2P. Appl Catal B 2021;295:120283.
- Yan Q, Chen X, Wei T, Wang G, Zhu M, Zhuo Y, Cheng K, Ye K, Zhu K, Yan J, Cao D, Li Y. Hierarchical edge-rich nickel phosphide nanosheet arrays as efficient electrocatalysts toward hydrogen evolution in both alkaline and acidic conditions. ACS Sustainable Chem Eng 2019;7(8):7804–11.
 Jiang N, Tang Q, Sheng M, You B, Jiang D, Sun Y. Nickel sulfides for
- [25] Jiang N, Tang Q, Sheng M, You B, Jiang D, Sun Y. Nickel sulfides for electrocatalytic hydrogen evolution under alkaline conditions: a case study of crystalline NiS, NiS2, and Ni3S2 nanoparticles. Catal Sci Technol 2016;6(4): 1077–84.
- [26] Li G, Ma Z, Li W, Nie Y, Pei L, Zhong J, Miao Q, Hu M-L, Wen X. Interfacial engineering of heterostructured Fe-Ni3S2/Ni(OH)2 nanosheets with tailored dband center for enhanced oxygen evolution catalysis. Dalton Trans 2022;51(45): 17391–6.
- [27] Zhang G, Feng Y-S, Lu W-T, He D, Wang C-Y, Li Y-K, Wang X-Y, Cao F-F. Enhanced catalysis of electrochemical overall water splitting in alkaline media by Fe doping in Ni3S2 nanosheet arrays. ACS Catal 2018;8(6):5431–41.
- [28] Zhang D, Mou H, Lu F, Song C, Wang D. A novel strategy for 2D/2D NiS/graphene heterostructures as efficient bifunctional electrocatalysts for overall water splitting. Appl Catal B 2019;254:471–8.
- [29] Liu T, Diao P, Lin Z, Wang H. Sulfur and selenium doped nickel chalcogenides as efficient and stable electrocatalysts for hydrogen evolution reaction: the importance of the dopant atoms in and beneath the surface. Nano Energy 2020;74: 104787.
- [30] M S, Vijay Rajyaguru Y, Kumar Rastogi C, Mp SA, M S, Khosla A, C M. Recent development of nickel based chalcogenides for hydrogen generation. Mater Today Proc 2023;73:316–22.
- [31] Wang B, Wang X, Zheng B, Yu B, Qi F, Zhang W, Li Y, Chen Y. NiSe2 nanoparticles embedded in CNT networks: scalable synthesis and superior electrocatalytic activity for the hydrogen evolution reaction. Electrochem Commun 2017;83:51–5.
- [32] Wu H, Lu X, Zheng G, Ho GW. Electrocatalysis: topotactic engineering of ultrathin 2D nonlayered nickel selenides for full water electrolysis (adv. Energy mater. 14/ 2018). Adv Energy Mater 2018;8(14):1870064.

- [33] Sun J, Meng X, Zhang Z, Li Z. Interface-induced phase engineering to boost intrinsic catalytic activity of nickel selenide for improved water/seawater hydrogen evolution. J Alloys Compd 2023;967:171815.
- [34] Maleki M, Barati Darband G, Sabour Rouhaghdam A, Andaveh R, Mohammad Kazemi Z. Mn-incorporated nickel selenide: an ultra-active bifunctional electrocatalyst for hydrogen evolution and urea oxidation reactions. Chem Commun 2022;58(21):3545–8.
- [35] Paseka I. Sorption of hydrogen and kinetics of hydrogen evolution on amorphous Ni-sx electrodes. Electrochim Acta 1993;38(16):2449–54.
- [36] Borucinsky Th, Rausch S, Wendt H. Smooth raney nickel coatings for cathodic hydrogen evolution by chemical gas phase reaction of nickel electrode surfaces J Appl Electrochem 1997;27(7):762–73.
- [37] Yuan F, Wang S, Yang G, Qin J, Chen M, Fan T, Ma J. Construction of nickel sulfide phase-heterostructure for alkaline hydrogen evolution reaction. J Colloid Interface Sci 2023;633:640–8.
- [38] Zheng X, Han X, Zhang Y, Wang J, Zhong C, Deng Y, Hu W. Controllable synthesis of nickel sulfide nanocatalysts and their phase-dependent performance for overall water splitting. Nanoscale 2019;11(12):5646–54.
- [39] Tan L, Yu J, Wang H, Gao H, Liu X, Wang L, She X, Zhan T. Controllable synthesis and phase-dependent catalytic performance of dual-phase nickel selenides on Ni foam for overall water splitting. Appl Catal B 2022;303:120915.
- [40] Yang W, Wang S, Luo W, Li L, Hao J, Shi W. Self-supported nickel sulfide derived from nickel foam for hydrogen evolution and oxygen evolution reaction: effect of crystal phase switching. Nanotechnology 2021;32(8):85710.
- [41] Tiwari AP, Yoon Y, Novak TG, An K-S, Jeon S. Continuous network of phase-tuned nickel sulfide nanostructures for electrocatalytic water splitting. ACS Appl Nano Mater 2019;2(8):5061–70.
- [42] Pan Y, Chen Y, Li X, Liu Y, Liu C. Nanostructured nickel sulfides: phase evolution, characterization and electrocatalytic properties for the hydrogen evolution reaction. RSC Adv 2015;5(127):104740–9.
- [43] Zeng W, Jiang Z, Gong X, Hu C, Luo X, Lei W, Yuan C. Atomic magnetic heating effect enhanced hydrogen evolution reaction of Gd@MoS2 single-atom catalysts. Small 2023;19(4):2206155.
- [44] Wang T, Tao L, Zhu X, Chen C, Chen W, Du S, Zhou Y, Zhou B, Wang D, Xie C, Long P, Li W, Wang Y, Chen R, Zou Y, Fu X-Z, Li Y, Duan X, Wang S. Combined anodic and cathodic hydrogen production from aldehyde oxidation and hydrogen evolution reaction. Nat Catal 2022;5(1):66–73.
- [45] Zhou W, Chen M, Guo M, Hong A, Yu T, Luo X, Yuan C, Lei W, Wang S. Magnetic enhancement for hydrogen evolution reaction on ferromagnetic MoS2 catalyst. Nano Lett 2020:20(4):2923–30.
- [46] Guo X, Wan X, Liu Q, Li Y, Li W, Shui J. Phosphated IrMo bimetallic cluster for efficient hydrogen evolution reaction. eScience 2022;2(3):304–10.
- [47] Tong S-S, Wang X-J, Li Q-C, Han X-J. Progress on electrocatalysts of hydrogen evolution reaction based on carbon fiber materials. Chin J Anal Chem 2016;44(9): 1447–57.
- [48] Koutavarapu R, Venkata Reddy C, Babu B, Reddy KR, Cho M, Shim J. Carbon cloth/transition metals-based hybrids with controllable architectures for electrocatalytic hydrogen evolution - a review. Int J Hydrogen Energy 2020;45 (13):7716–40.
- [49] Banerjee R, Ghosh D, Kirti, Chanda D Kr, Mondal A, Srivastava DN, Biswas P. Nickel sulphide decorated nitrogen rich ordered mesoporous carbon (NOMC) as an efficient catalyst for the electrocatalytic oxidation of urea in alkaline medium. Electrochim Acta 2022;408:139920.
- [50] Zhu W, Yue X, Zhang W, Yu S, Zhang Y, Wang J, Wang J. Nickel sulfide microsphere film on Ni foam as an efficient bifunctional electrocatalyst for overall water splitting. Chem Commun 2016;52(7):1486–9.
- [51] Lin T-W, Liu C-J, Dai C-S. Ni3S2/Carbon nanotube nanocomposite as electrode material for hydrogen evolution reaction in alkaline electrolyte and enzyme-free glucose detection. Appl Catal B 2014;154(155):213–20.
- [52] Yang YJ, Hu X. Nanoporous Ni3S2 film on Ni foam as highly efficient electrocatalyst for hydrogen evolution in acidic electrolyte. Russ J Electrochem 2019;55(2):88–96.
- [53] Ho TA, Bae C, Nam H, Kim E, Lee SY, Park JH, Shin H. Metallic Ni3S2 films grown by atomic layer deposition as an efficient and stable electrocatalyst for overall water splitting. ACS Appl Mater Interfaces 2018;10(15):12807–15.
- [54] Zhang D, Li J, Luo J, Xu P, Wei L, Zhou D, Xu W, Yuan D. Ni3S2 nanowires grown on nickel foam as an efficient bifunctional electrocatalyst for water splitting with greatly practical prospects. Nanotechnology 2018;29(24):245402.
- [55] Jiang N, Tang Q, Sheng M, You B, Jiang D, Sun Y. Nickel sulfides for electrocatalytic hydrogen evolution under alkaline conditions: a case study of crystalline NiS, NiS2, and Ni3S2 nanoparticles. Catal Sci Technol 2016;6(4): 1077–84.
- [56] Zhou W, Zhao J, Guan J, Wu M, Li G-R. Ni3S2 in situ grown on Ni foam coupled with nitrogen-doped carbon nanotubes as an efficient electrocatalyst for the hydrogen evolution reaction in alkaline solution. ACS Omega 2019;4(23): 20244–51.
- [57] Poudel YR, Zhao X, Jungjohann KL, Thapa A, Guo R, Li W. Ni3S2 nanowires filled carbon nanotubes of ultra-high quality: synthesis methods, structure, and electrical properties. Diam Relat Mater 2022;127:109156.
- [58] Thapa A, Jungjohann KL, Wang X, Li W. Improving field emission properties of vertically aligned carbon nanotube arrays through a structure modification. J Mater Sci 2020;55(5):2101–17.
- [59] Anantharaj S, Noda S, Jothi VR, Yi S, Driess M, Menezes PW. Strategies and perspectives to catch the missing pieces in energy-efficient hydrogen evolution reaction in alkaline media. Angew Chem Int Ed 2021;60(35):18981–9006.

ARTICLE IN PRESS

International Journal of Hydrogen Energy xxx (xxxx) xxx

- [60] Yu SH, Chua DHC. Toward high-performance and low-cost hydrogen evolution reaction electrocatalysts: nanostructuring cobalt phosphide (CoP) particles on carbon fiber paper. ACS Appl Mater Interfaces 2018;10(17):14777–85.
- [61] Bao F, Kemppainen E, Dorbandt I, Bors R, Xi F, Schlatmann R, van de Krol R, Calnan S. Understanding the hydrogen evolution reaction kinetics of electrodeposited nickel-molybdenum in acidic, near-neutral, and alkaline conditions. Chemelectrochem 2021;8(1):195–208.
- [62] Li J, Zhou C, Mu J, Yang E-C, Zhao X-J. In situ synthesis of molybdenum carbide/N-doped carbon hybrids as an efficient hydrogen-evolution electrocatalyst. RSC Adv 2018;8(31):17202–8.
- [63] Subramanya B, Ullal Y, Shenoy SU, Bhat DK, Hegde AC. Novel Co-Ni-graphene composite electrodes for hydrogen production. RSC Adv 2015;5(59):47398–407.
- [64] Han Y, Mao X, Yan X, Wu Q, Xu H, Fang Q, Jia Y, Yao X, Li Q, Du A. Carbon nanotubes encapsulated transition metals for efficient hydrogen evolution reaction: coupling effect of 3d orbital and π-bond. Mater Today Chem 2023;30:101573.
- [65] Chen C, Wen M, Cheng T, Tian Y, Zhang X, Hou B. Accessible active sites activated by nano cobalt antimony oxide @ carbon nanotube composite electrocatalyst for highly enhanced hydrogen evolution reaction. Int J Hydrogen Energy 2023;48(21): 7719–36.
- [66] Nangan S, Natesan T, Sukmas W, Okhawilai M, Justice Babu K, Tsuppayakorn-aek P, Bovornratanaraks T, Wongsalam T, Vimal V, Uyama H, Al-Enizi AM, Kansal L, Sehgal SS. Waste plastics derived nickel-palladium alloy filled carbon nanotubes for hydrogen evolution reaction. Chemosphere 2023;341:139982.
- [67] Lasia A. Mechanism and kinetics of the hydrogen evolution reaction. Int J Hydrogen Energy 2019;44(36):19484–518.
- [68] Trasatti S, Petrii OA. Real Surface Area Measurements in Electrochemistry 1991;63 (5):711–34.
- [69] McCrory CCL, Jung S, Ferrer IM, Chatman SM, Peters JC, Jaramillo TF. Benchmarking hydrogen evolving reaction and oxygen evolving reaction electrocatalysts for solar water splitting devices. J Am Chem Soc 2015;137(13): 4347–57.
- [70] Zhang D, Mou H, Lu F, Song C, Wang D. A novel strategy for 2D/2D NiS/graphene heterostructures as efficient bifunctional electrocatalysts for overall water splitting. Appl Catal B 2019;254:471–8.
- [71] Li DY, Liao LL, Zhou HQ, Zhao Y, Cai FM, Zeng JS, Liu F, Wu H, Tang DS, Yu F. Highly active non-noble electrocatalyst from Co2P/Ni2P nanohybrids for PHuniversal hydrogen evolution reaction. Materials Today Physics 2021:16:100314.

- [72] Ma W, Li D, Liao L, Zhou H, Zhang F, Zhou X, Mo Y, Yu F. High-performance bifunctional porous iron-rich phosphide/nickel nitride heterostructures for alkaline seawater splitting. Small 2023;19(19):2207082.
- [73] Rabia M, Shaban M, Adel A, Abdel-Khaliek AA. Effect of plasmonic Au nanoparticles on the photoactivity of polyaniline/indium tin oxide electrodes for water splitting. Environ Prog Sustain Energy 2019;38(5):13171.
- [74] Shaban M, Kholidy I, Ahmed GM, Negem M, Abd El-Salam HM. Cyclic voltammetry growth and characterization of Sn-Ag alloys of different nanomorphologies and compositions for efficient hydrogen evolution in alkaline solutions. RSC Adv 2019; 9(39):22389–400.
- [75] Kakaei K, Ostadi Z. Nickel nanoparticles coated on the exfoliated graphene layer as an efficient and stable catalyst for oxygen reduction and hydrogen evolution in alkaline media. Mater Res Express 2020;7(5):55504.
- [76] Lin T-W, Liu C-J, Dai C-S. Ni3S2/Carbon nanotube nanocomposite as electrode material for hydrogen evolution reaction in alkaline electrolyte and enzyme-free glucose detection. Appl Catal B 2014;154(155):213–20.
- [77] Sing KSW. Reporting physisorption data for gas/solid systems with special reference to the determination of surface area and porosity. Recommendations 1984) 1985;57(4):603–19.
- [78] Dinesh M, Muthumalai K, Haldorai Y, Thangavelu Rajendra Kumar R. MoS2 nanosheets decorated multi-walled carbon nanotube composite electrocatalyst for 4-nitrophenol detection and hydrogen evolution reaction. Electroanalysis 2020;32 (11):2571–80.
- [79] Li F, Li J, Lin X, Li X, Fang Y, Jiao L, An X, Fu Y, Jin J, Li R. Designed synthesis of multi-walled carbon nanotubes@Cu@MoS2 hybrid as advanced electrocatalyst for highly efficient hydrogen evolution reaction. J Power Sources 2015;300:301–8.
- [80] Hu H, Tian M, Li F, Gao L, Xu N, Hu Y, Long X, Ma J, Jin J. Phosphorus dual-doped MoO2 nanosheet/multiwalled carbon nanotube hybrid as efficient electrocatalyst for hydrogen evolution. Chemelectrochem 2018;5(18):2660–5.
- [81] Attatsi IK, Zhong H, Du J, Zhu W, Li M, Liang X. Multiwalled carbon nanotube conjugates of pyrene-substituted metalloporphyrins as electrocatalysts for hydrogen evolution reactions. Inorg Chim Acta 2020;503:119398.
- [82] Nguyen TK, Bannov AG, Popov MV, Yun J-W, Nguyen AD, Kim YS. Hightemperature-treated multiwall carbon nanotubes for hydrogen evolution reaction. Int J Hydrogen Energy 2018;43(13):6526–31.